Dynamic Simulation of Gyroscopic Rigid Rotor with Anisotropy of Elastic Support Restoring and Damping Characteristics

Zharilkassin Iskakov[(✉)] [iD], Azizbek Abduraimov [iD], and Aziz Kamal [iD]

Joldasbekov Institute of Mechanics and Engineering, Almaty, Kazakhstan
`iskakov53@mail.ru`

Abstract. This paper considers a gyroscopic rigid rotor with restoring and damping characteristics of an elastic support. Differential equations of the rotor motion, which take into account the anisotropy of stiffness and damping, are solved analytically by the harmonic balance method. It is found that if the linear stiffness of the elastic support material differs in two mutually perpendicular directions, there are two critical velocities and corresponding resonance regions. Each critical velocity is defined by two resonance curves, the principal direction and the perpendicular direction, respectively. The area limited by the principal direction resonance curve is larger than the area limited by the second direction resonance curve. Linear damping or non-linear cubic damping suppresses the maximum amplitudes of these resonant curves. If damping acts only in one direction, then its effect is observed in the resonance curves of the corresponding critical velocity. In the case of the presence of a non-linear component of the rigidity of the support material, the resonance curves of the main directions are accompanied by jumps. Combined linear and non-linear cubic damping suppresses the oscillation amplitude more significantly than linear damping. The equations of rotor motion were also solved numerically and the results are in good agreement with the results of the analytical solution at the initial stage of time.

Keywords: Dynamic simulation · Gyroscopic rotor · Stiffness anisotropy · Damping anisotropy · Non-linear damping

1 Introduction

Although rotor machines have been profoundly researched for a long time, and the extensive array of literature has been focused on investigation of their dynamics, there are still many problems related to vibrations that occur during machine start-up, operation and shut-down. These problems are caused, in particular, by uneven weight distribution, faults in the supporting structure and the bearings. The restoring and damping properties and characteristics of the support material are very important in order to stabilize the motion. In addition to optimal selection of stiffness and optimal damping of the elastic support, the precise design of the support elements must be reasonably determined to

ensure reliable machine operation. A precise dynamic calculation of the machine allows the correct analysis of the elastic support to be carried out.

It is known that linear oscillation damping occurs only near critical speeds, and non-linear cubic damping, in contrast to linear damping, not only significantly suppresses the maximum resonant amplitude of the oscillations, but also keeps the vibration isolation of the system in a wide range of speed of the machine shaft, eliminates jumping effects [1–9].

Non-linear cubic damping along with the expansion of the vibration isolation area is also used to control the rotor resonant oscillations with large amplitudes and to go outside of the area of instability with the Sommerfeld effects [8] or to weaken and eliminate these effects [4–10].

In [11] it is demonstrated how the cubic nonlinearity of damping can be distinguished from other types of nonlinearity, an algorithm for estimating the parameter of cubic damping nonlinearity is developed.

The vertical deviation of a shaft axis, for example in a gyroscopic rotor, due to the uneven stiffness and damping of the resilient support material will cause uneven wear of the gearing and shocks in the drive train. Any resilient support material stiffness and damping variation consists of the sum of such variations in two directions: opposite to each other and mutually perpendicular. With the asymmetry of rigidity, there is a critical velocity corresponding to the mode of increasing the speed and a critical velocity that occurs when the speed of rotation of the shaft decreases [9]. The support stiffness variations in two mutually perpendicular directions result in two critical velocities and, correspondingly, two resonance regions with jump effects in the presence of a non-linear stiffness component instead of one critical velocity and a resonance region [8, 10], which is undesirable. This warrants the importance of the dynamic study of the of a gyroscopic rigid rotor at anisotropy of stiffness and damping of the support material needed in order to afjust and select the support material with optimal stiffness and damping properties, resulting in the stable operation of the machine.

2   Equations of Motion. Frequency Responses

We consider a harmonically forced ideal rotary system consisting of a disk, a shaft, and a support structure (see Fig. 1). The disk has the mass m, the moment of inertia relative to its rotational axis J_P and the moment of inertia relative to its diametrical axis J_T. It is fixed without skewing on the free end of the rigid shaft. The shaft has the length L and is mounted vertically by means of a bottom hinged and an upper elastic support. The distance between the supports is l_0. The speed of the shaft rotation $\dot{\varphi}$, is so high that the rotor can be considered as a gyroscope. The position of the geometric center of disk S in the stationary coordinate system $Oxyz$ is determined by the coordinates and the position of the shaft in space is determined by the Euler angles α, β nd the angle of rotation φ. Then we denote the coordinates of the disk center of mass m as x_m and y_m. We also assume that the linear eccentricity e lies in the axis N of the coordinate system $ONKZ$. If we restrict ourselves to small deviations of the rotor axis, then the coordinate z can be deemed as equal to $z = L = $ const and excluded from consideration.

Let us express the projections of the angular velocity of the rotor in the coordinate axes of the system $ONKZ$, the coordinates of the disk center of mass and the coordinates of
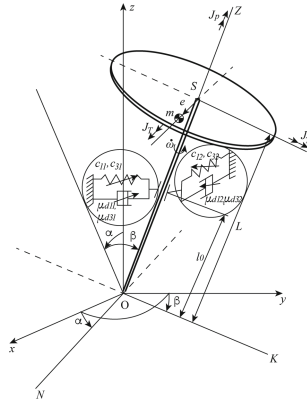
Fig. 1. Structural diagram of the rotor.

the upper support through the angular coordinates α, β and φ. Thus, we find expressions for the kinetic energy of the disk, the potential energy, and the generalized Rayleigh function, given the anisotropy of the stiffness and damping of the elastic support in two mutually perpendicular directions, and the projections of the momentum of gravity acting on the rotor.

The natural frequencies (critical speeds) of a non-damped rotor system [8]:

$$\omega_{1,2} = \sqrt{\tilde{b} \big/ 2 \mp \sqrt{\tilde{b}^2 \big/ 4 - \tilde{c}}}, \tag{1}$$

where

$$\tilde{b} = \frac{(J_T + mL^2)\left[(c_{11}l_0^2 - mgL) + (c_{12}l_0^2 - mgL)\right]}{(J_T + mL^2)^2 - J_P^2}, \tilde{c} = \frac{(c_{11}l_0^2 - mgL)(c_{12}l_0^2 - mgL)}{(J_T + mL^2)^2 - J_P^2}, \tag{2}$$

For numerical calculations, some geometric and dynamic parameters of the gyroscopic rotor system are borrowed from the experimental setup used in [5]: $L = 0.46$ m, $l_0 = 0.33$ m, $m = 2$ kg, $c_{11} = 2\ 10^4$ N/m, $c_{12} = 2.4\ 10^4$ N/m, $J_T = 0.090$ kgm^2, $J_P = 0.011$ kgm^2, $e = 0.0193$ m.

The intrinsic angular velocity of shaft rotation ω_1, calculated using formula (1) and taking into account expressions (2), in the interval of difference of natural frequencies [64.95 s^{-1}, 64.48 s^{-1}], can be approximately considered constant and equal to $\omega_1 = 65\ s^{-1}$. This allows ω_1 to be used in the process of bringing the system parameters into a dimensionless form.

Let us introduce the following dimensionless parameters of the system:

$$l = l_0 \big/ L; \bar{t} = t\omega_1; \bar{J}_p = J_p \big/ (mL^2); \bar{J}_T = J_T \big/ (mL^2); J_{p1} = \bar{J}_p \big/ (1 + \bar{J}_T);$$
$$\overline{G} = g \big/ (L\omega_1^2); e_r = e/[L(1 + \bar{J}_T)]; \overline{C}_{11} = c_{11} \big/ (m\omega_1^2); \overline{C}_{12} = c_{12} \big/ (m\omega_1^2);$$
$$C_{31} = c_{31}l_0^4 \big/ \left[mL^2\omega_1^2(1 + \bar{J}_T) \right]; C_{32} = c_{32}l_0^4 \big/ \left[mL^2\omega_1^2(1 + \bar{J}_T) \right]; \tag{3}$$
$$\mu_{11} = \mu_{d11} \big/ \left[mL^2\omega_1(1 + \bar{J}_T) \right]; \mu_{12} = \mu_{d12} \big/ \left[mL^2\omega_1(1 + \bar{J}_T) \right];$$
$$\mu_{31} = \mu_{d31}\omega_1 \big/ \left[mL^2(1 + \bar{J}_T) \right]; \mu_{32} = \mu_{d32}\omega_1 \big/ \left[mL^2(1 + \bar{J}_T) \right];$$

where c_{11}, c_{12} are linear stiffness coefficients, c_{31}, c_{32} are non-linear stiffness coefficients of the support in mutually perpendicular directions, μ_{d11}, μ_{d12} are linear viscous damping coefficients, μ_{d31}, μ_{d32} are non-linear cubic viscous damping coefficients in mutually perpendicular directions, and ω_1 is the first natural frequency (first critical speed) of the non-damped rotor system.

In the absence of anisotropy of elasticity and damping of the support material, this property can be created using the following methodology. In a steel spring support, the unevenness of its elastic properties can be realized by adjusting the tension of the springs in opposite directions or in orthogonal directions. Viscoelastic materials: rubber, rubber, etc. simultaneously have a damping property. Figure 2 shows the arrangement of viscoelastic plates on four support cells in cases of uneven of stiffness and damping in opposite directions (Fig. 2a) and orthogonal directions (Fig. 2b).

a   b
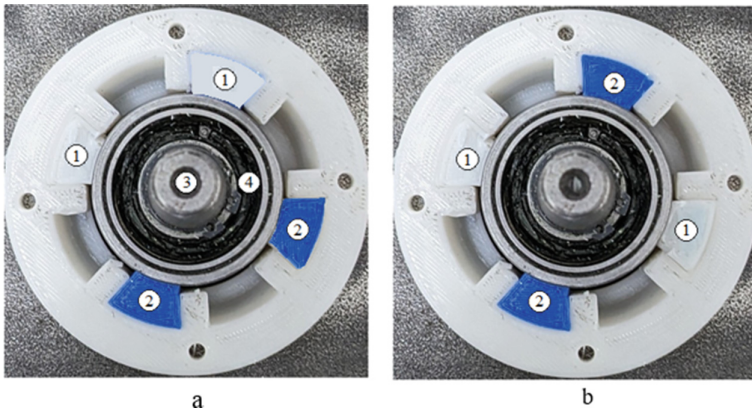
Fig. 2. Elastic supports with unevenness of stiffness and damping in opposite directions (a) and in orthogonal directions (b): 1 - HIPS plate (high impact polystyrene), 2 – Bflex plate, 3 - shaft, 4 – bearing

Non-linear differential equations of the rotor motion, derived from the Lagrange equations of the second kind, using (3), the assumptions of the second and higher orders of smallness relatively to α, β, their derivatives, and their combinations $\varphi'' \ll \Omega^2$, and

$\overline{J}_p \ll \overline{J}_T$ can be represented in dimensionless form:

$$\alpha'' + J_{p1}\Omega\beta' + \mu_{11}\alpha' + \mu_{31}\alpha'^3 + \omega_{n1}^2\alpha + C_{31}\alpha^3 = e_r\Omega^2\cos\Omega\bar{t},$$
$$\beta'' - J_{p1}\Omega\alpha' + \mu_{12}\beta' + \mu_{32}\beta'^3 + \omega_{n2}^2\beta + C_{32}\beta^3 = e_r\Omega^2\sin\Omega\bar{t},$$

(4)

Where

$$\omega_{n1} = \sqrt{(\overline{C}_{11}l^2 - \overline{G})/(1 + \overline{J}_T)}$$

(5)

is the dimensionless natural frequency of the rotor system (4) at, $\overline{C}_1 = \overline{C}_{11}$

$$\omega_{n2} = \sqrt{(\overline{C}_{12}l^2 - \overline{G})/(1 + \overline{J}_T)}$$

(6)

- is the dimensionless natural frequency of the rotor system (4) at $\overline{C}_1 = \overline{C}_{12}$, where it is assumed that $\overline{J}_T \gg \overline{J}_p$.

Values α and β are generalized coordinates, and when these values are low, the harmonic oscillations at the frequency of the forcing momentum of centrifugal force of inertia prevail in solutions of system (4). Then we can proceed with solution of system (4) in the following form:

$$\alpha = A\cos(\Omega\bar{t} + \gamma), \beta = B\sin(\Omega\bar{t} + \delta),$$

(7)

where A, B are oscillation amplitudes in two mutually perpendicular directions, γ, δ are phase displacement angles between the oscillations of angular coordinates and the projections of the centrifugal momentum of centrifugal inertia.

Substituting expressions (7) into system (4), using some trigonometric identities and equating only the coefficients at functions $\cos\Omega\bar{t}$ and $\sin\Omega\bar{t}$, we obtain a system of four equations with respect to four variables A, B, γ, δ. From here, introducing the following notations:

$$C_A = \left(\omega_{n1}^2 - \Omega^2\right)A + 0.75C_{31}A^3, \mu_A = \mu_{11}\Omega A + 0.75\mu_{31}\Omega^3A^3, J_{PA} = J_{p1}\Omega^2A,$$
$$C_B = \left(\omega_{n2}^2 - \Omega^2\right)B + 0.75C_{32}B^3, \mu_B = \mu_{12}\Omega B + 0.75\mu_{32}\Omega^3B^3, J_{PB} = J_{p1}\Omega^2B,$$
$$e_\Omega = e_r\Omega^2.$$

(8)

let us present the expressions for the amplitude-frequency dependences as follows:

$$e_\Omega^2\left\{\begin{array}{l} \left\{C_A\left(C_B^2 + \mu_B^2\right) + J_{PB}[J_{PA}(J_{PB} - C_B) + \mu_A\mu_B - C_AC_B]\right\}^2 + \\ \left\{\mu_A\left(C_B^2 + \mu_B^2\right) + J_{PB}[J_{PA}\mu_B - (\mu_BC_A + \mu_AC_B)]\right\}^2 \end{array}\right\}$$
$$= \left\{\left(C_A^2 + \mu_A^2\right)\left(C_B^2 + \mu_B^2\right) + J_{PA}J_{PB}[2(\mu_A\mu_B - C_AC_B) + J_{PA}J_{PB}]\right\}^2,$$

(9)

$$
e_{\Omega}^2 \left\{ \begin{array}{l} \left\{ J_{PA}[J_{PA}J_{PB} + \mu_A\mu_B - C_A(C_B + J_{PB})] + C_B\left(C_A^2 + \mu_A^2\right) \right\}^2 + \\ \left\{ J_{PA}[J_{PB}\mu_A - (\mu_A C_B + \mu_B C_A)] + \mu_B\left(C_A^2 + \mu_A^2\right) \right\}^2 \end{array} \right\} \tag{10}
$$
$$
= \left\{ \left(C_A^2 + \mu_A^2\right)\left(C_B^2 + \mu_B^2\right) + J_{PA}J_{PB}[2(\mu_A\mu_B - C_A C_B) + J_{PA}J_{PB}] \right\}^2,
$$

and let us present the expressions for phase-frequency dependencies as follows:

$$
\tan\gamma = -\frac{\mu_A\left(C_B^2 + \mu_B^2\right) + J_{PB}[J_{PA}\mu_B - (\mu_B C_A + \mu_A C_B)]}{C_A\left(C_B^2 + \mu_B^2\right) + J_{PB}[J_{PA}(J_{PB} - C_B) + \mu_A\mu_B - C_A C_B]},
$$
$$
\tan\delta = -\frac{J_{PA}[J_{PB}\mu_A - (\mu_A C_B + \mu_B C_A)] + \mu_B\left(C_A^2 + \mu_A^2\right)}{J_{PA}[J_{PA}J_{PB} + \mu_A\mu_B - C_A(C_B + J_{PB})] + C_B\left(C_A^2 + \mu_A^2\right)}. \tag{11}
$$

3   Results. Amplitude-Frequency Dependencies

Calculations using the formulas (1), (2) and (3) gives the following values of dimensionless parameters: $l = 0.72$; $\overline{J}_p = 0.026$; $\overline{J}_T = 0.213$; $\overline{G} = 0.0051$; $\overline{C}_{11} = 2.37$; $\overline{C}_{12} = 2.84$; $e_r = 0.0346$; $J_{p1} = 0.021$; $\omega_{n1} = 1$, $\omega_{n2} = 1.1$. Dimensionless parameters $C_{31} = C_{32} = 0.1$; $\mu_{11} = 0.01, 0.02, 0.04$; $\mu_{12} = 0.01, 0.02, 0.04$; $\mu_{31} = 0.01, 0.02, 0.04$; $\mu_{32} = 0.01, 0.02, 0.04$ were chosen out of the right physical consideration. Since, at values $C_{31} = C_{32} = 0.1$ and $\mu_{3i} = 0.01, 0.02$ $(i = 1, 2)$ and $\mu_{3i} = 0.01, 0.02$ $(i = 1, 2)$, the slopes of the resonance curves and jumping effects will be well noticed, at $\mu_{3i} = 0.04$ $(i = 1, 2)$, these effects will already be eliminated.

The results of calculations using formulas (9) and (10) are shown in Figs. 3, 4, 5, 6, 7, 8, 9, 10, 11, 12, 13, and 14. From these plots, the one can see two critical velocities and two resonance regions corresponding to the values of the linear stiffness of the support material in two mutually perpendicular directions.
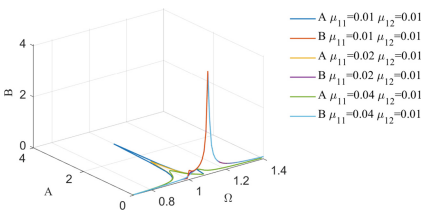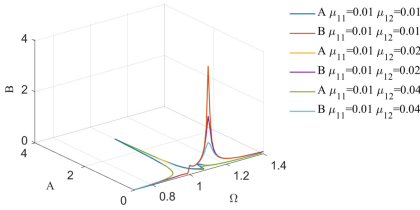

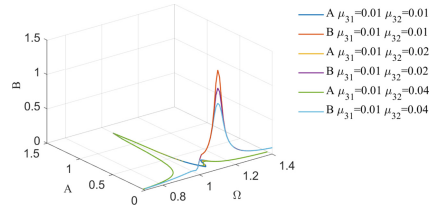**Fig. 3.** Amplitude-frequency dependences at various values of μ_{11} and constant value of $\mu_{12} = 0.01$.
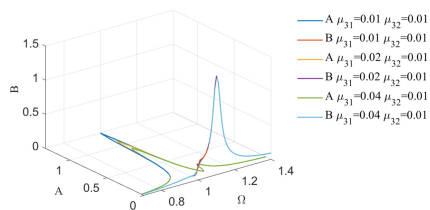
Fig. 4. Amplitude-frequency dependences at various values of μ_{31} and constant values of $\mu_{32} = 0.01$ of $\mu_{11} = \mu_{12} = 0.01$.

For each of the two mutually perpendicular directions there are two resonant regions. At each critical velocity, the resonant region of the main direction is larger in size than for the second direction. Increase of the linear damping coefficient or the non-linear
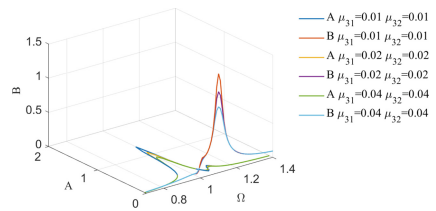
Fig. 5. Amplitude-frequency dependences at constant value of $\mu_{11} = 0.01$ and various values of μ_{12}.

Fig. 6. Amplitude-frequency dependences at constant values of $\mu_{31} = 0.01$ and $\mu_{11} = \mu_{12} = 0.01$ and various values of μ_{32}.
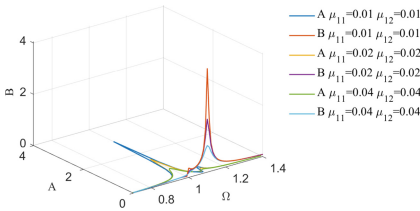
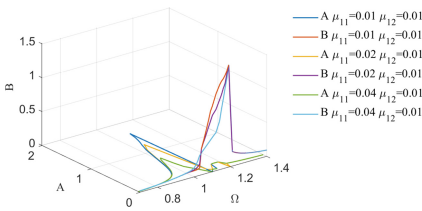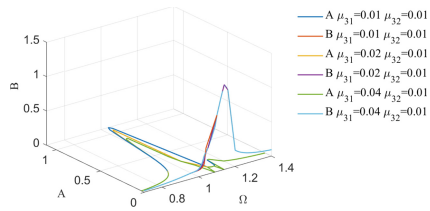**Fig. 7.** Amplitude-frequency dependences at various values of $\mu_{11} = \mu_{12}$.

Fig. 8. Amplitude-frequency dependences at various values of $\mu_{31} = \mu_{32}$ and constant value of $\mu_{11} = \mu_{12} = 0.01$.

cubic damping coefficient (when the linear damping value is constant) for one of the directions suppresses the resonance curves caused by vibrations of the given direction and vibrations of the perpendicular direction, but corresponding to the given critical velocity. A comparative analysis shows that the combined linear and non-linear cubic damping suppresses the maximum amplitudes of the resonance curves more significantly than linear damping.

The graphs in Figs. 9, 10, 11, 12, 13, and 14 show that with irregularities of linear stiffness in mutually perpendicular directions and the presence of a nonlinear cubic component of the stiffness of the flexible support material, the resonant curves of the main directions have four jumping effects (the figures show two jumping effects). They can be eliminated more efficiently with an increase in the magnitude of joint linear and nonlinear cubic damping (see Figs. 10, 12 and 14) compared to linear damping (see Figs. 9, 11 and 13). It is known that with the isotropy of the linear stiffness of the support material, the resonance curve can have only two jumping effects.

To verify the reliability of the results obtained, the results of analytical and numerical solutions of the equations of motion (4) were compared (see Figs. 15 and 17).
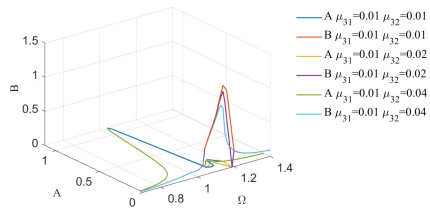

Fig. 9. Amplitude-frequency dependences at $C_{31} = C_{32} = 0.1$, various values of μ_{11} and constant value of $\mu_{12} = 0.01$.
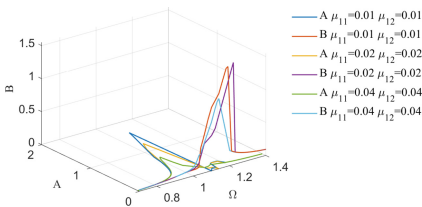

Fig. 10. Amplitude-frequency dependences at $C_{31} = C_{32} = 0.1$, various values of μ_{31} and constant values of $\mu_{32} = 0.01$ of $\mu_{11} = \mu_{12} = 0.01$.
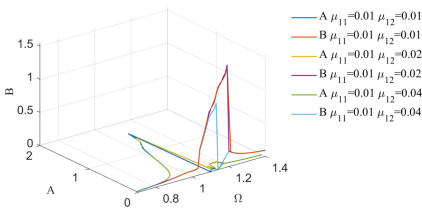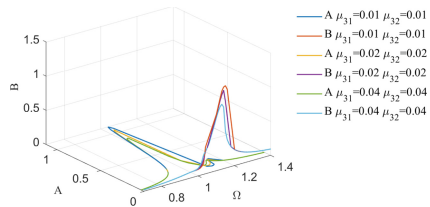

Fig. 11. Amplitude-frequency dependences at $C_{31} = C_{32} = 0.1$, constant value of $\mu_{11} = 0.01$ and various values of μ_{12}.

Fig. 12. Amplitude-frequency dependences at $C_{31} = C_{32} = 0.1$, constant values of $\mu_{31} = 0.01$ and $\mu_{11} = \mu_{12} = 0.01$ and various values of μ_{32}.


Fig. 13. Amplitude-frequency dependences at $C_{31} = C_{32} = 0.1$, various values of $\mu_{11} = \mu_{12}$.


Fig. 14. Amplitude-frequency dependences at $C_{31} = C_{32} = 0.1$, various values of $\mu_{31} = \mu_{32}$ and constant value of $\mu_{11} = \mu_{12} = 0.01$.

Comparative analysis shows the proximity of these results at the initial stage of time and a decrease in their convergence over time, this is especially noticeable in the graphs $\beta = \beta(\bar{t})$ (see Fig. 17). The suppression of the amplitudes of the angular coordinate waveforms obtained by the numerical method, as the value of μ_{32} increases (see Figs. 16 and 18), also proves the correctness of the analytically obtained conclusions. Analytical and numerical solutions of Eqs. (4) were carried out for the following parameters: $\Omega = 1.0067$; $C_{31} = C_{32} = 0$; $\mu_{31} = 0.01, 0.02, 0.04$; $\mu_{32} = 0.01$; $\mu_{11} = \mu_{12} = 0.01$.
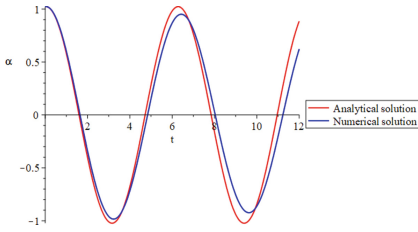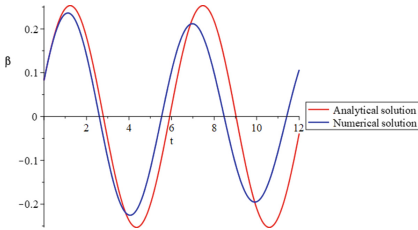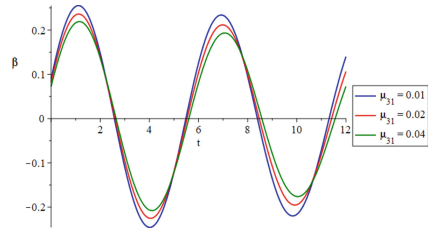
Fig. 15. Oscillograms $\alpha = \alpha\left(\bar{t}\right)$ plotted based on analytical and numerical solutions of equations at values $\mu_{31} = 0.02$, $\mu_{32} = 0.01$ and $\mu_{11} = \mu_{12} = 0.01$.
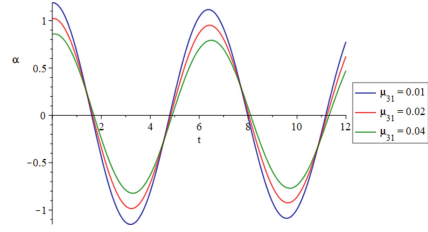
Fig. 16. Oscillograms $\alpha = \alpha\left(\bar{t}\right)$ plotted based on numerical solutions of equations of motion at various values of μ_{31} and constant values of $\mu_{32} = 0.01$ and $\mu_{11} = \mu_{12} = 0.01$.

Fig. 17. Oscillograms $\beta = \beta\left(\bar{t}\right)$, plotted based on analytical and numerical solutions of equations of motion at values $\mu_{31} = 0.02$, $\mu_{32} = 0.01$ and $\mu_{11} = \mu_{12} = 0.01$.

Fig. 18. Oscillograms $\beta = \beta\left(\bar{t}\right)$ plotted based on numerical solutions of equations of motion at various values of μ_{31} and constant values of $\mu_{32} = 0.01$ and $\mu_{11} = \mu_{12} = 0.01$.

4 Conclusion

The differential equations of motion of a gyroscopic rigid rotor taking into account the anisotropy of restoring and damping properties of the elastic support material are constructed and solved analytically by the harmonic balance method.

If the linear stiffness of the elastic support material differs in two mutually perpendicular directions, two critical velocities and corresponding resonant regions are found.

At each critical velocity, the area of the resonance curve of the main direction is greater than the area of the resonance curve of the perpendicular direction.

In the case of the presence of a non-linear component of the rigidity of the support material, the resonant phenomena of the main directions are accompanied by jumping effects.

Joint linear and non-linear damping suppresses the resonance amplitudes of each direction more significantly than linear damping.

The results of analytical and numerical solutions ща the equations of motion of the rotor are in good agreement with each other at the initial stage of time.

References

1. Lang, Z.Q., Jing, X.J., Billings, S.A., Tomilinson, G.R., Peng, Z.K.: Significant effects of nonlinear damping on vibration isolation. J. Sound. Vib. **323**, 352–365 (2009)
2. Peng, Z.K., Mengand Lang, Z.Q., Zhang, W.M., Chu, F.L.: Study of the effects of cubic non-linear damping on vibration isolations using Harmonic Balance Method. Int. J. Non-lin. Mech. **47**(10), 1065–1166 (2012)
3. Xiao, Z.L., Jing, X., Cheng, L.: The transmissibility of vibration isolators with cubic non-linear damping under both force and base excitations. J. Sound. Vib. **332**(5), 1335–1354 (2013)
4. Iskakov, Zh.: Resonant Oscillations of a Vertical Hard Gyroscopic Rotor with Linear and Non-linear Damping. Advances in Mechanism and Machine Science – Mechanisms and Machine Science, vol. 73, pp. 3353–3361 (2019). https://doi.org/10.1007/978-3-030-20131-9_331
5. Iskakov, Z., Bissembayev, K., Jamalov, N.: Resonance vibrations of a gyroscopic rotor with linear and nonlinear damping and nonlinear stiffness of the elastic support in interaction with a non-ideal energy source. Mech. Syst. Signal Pr. **170**, 108773 (2022)
6. Iskakov, Z., Jamalov, N., Abduraimov, A.: Nonstationary Resonant Oscillations of a Gyroscopic Rigid Rotor with Nonlinear Damping and Non-ideal Energy Source. In: Khang, N.V., Hoang, N.Q., Ceccarelli, M. (eds.) ASIAN MMS 2021. MMS, vol. 113, pp. 755–763. Springer, Cham (2022). https://doi.org/10.1007/978-3-030-91892-7_72
7. Mofidian, S.M.M., Bardaweel, H.: Displacement transmissibility evaluation of vibration isolation system employing nonlinear-damping and nonlinear-stiffness elements. J. Vib. Control **24**(18), 4247–4259 (2018)
8. Iskakov, Z., Bissembayev, K., Jamalov, N., Kamal, A.: Dynamic modeling of a non-ideal gyroscopic rotor system with nonlinear damping and nonlinear rigidity of an elastic support. Adv. Mech. Eng. **14**(7), 1–31 (2022)
9. Bharti, S.K., et al.: Sommerfeld effect at forward and backward critical speeds in a rigid rotor shaft system with anisotropic supports. J. Sound. Vib. **442**, 330–349 (2019)
10. Iskakov, Z., Jamalov, N., Abduraimov, A.: Non-stationary resonance transition of the gyroscopic rigid rotor with nonlinear damping and non-ideal energy source. In: Vincenzo, N., Gasparetto, A., Quaglia, G. (eds.) IFToMM Italy 2022: Advances in Italian Mechanism Science, Mechanisms and Machine Science, vol. 122, pp. 114–122. Springer, Cham (2022). https://doi.org/10.1007/978-3-031-10776-4_14
11. Chatterjee, A., Chintha, H.P.: Identification and parameter estimation of cubic nonlinear damping using harmonic probing and volterra series. Int. J. Mech. Sci. **125**, 103518 (2020)